Machine-learning techniques for fast and accurate holographic particle tracking

Mark D. Hannel,[1] Aidan Abdulali,[2] Michael O'Brien,[1] and David G. Grier[1]

[1] *Department of Physics and Center for Soft Matter Research, New York University, New York, NY 10003*
[2] *Packer Collegiate Institute, Brooklyn, NY 11201*

Quantitative analysis of holographic microscopy images yields the three-dimensional positions of micrometer-scale colloidal particles with nanometer precision, while simultaneously measuring the particles' sizes and refractive indexes. Extracting this information begins by detecting and localizing features of interest within individual holograms. Conventionally approached with heuristic algorithms, this image analysis problem can be solved faster and more generally with machine-learning techniques. We demonstrate that two popular machine-learning algorithms, cascade classifiers and deep convolutional neural networks (CNN), can solve the particle-tracking problem orders of magnitude faster than current state-of-the-art techniques. Our CNN implementation localizes holographic features precisely enough to bootstrap more detailed analyses based on the Lorenz-Mie theory of light scattering. The wavelet-based Haar cascade performs less well at detecting and localizing particles, but is so computationally efficient that it creates new opportunities for applications that emphasize speed and low cost. We demonstrate its use as a real-time targeting system for holographic optical trapping.

INTRODUCTION: HOLOGRAPHIC PARTICLE CHARACTERIZATION

Holographic particle characterization [1] uses quantitative analysis of holographic video microscopy images to measure the size, shape, composition and three-dimensional position of individual colloidal particles in dispersions. Performing holographic characterization measurements on a stream of dispersed particles provides insights into the composition of the dispersion as a whole that cannot be obtained in any other way. This technique has been demonstrated on homogeneous and heterogeneous [2, 3] dispersions of colloidal spheres, and has been extended to work for colloidal clusters [4, 5], and aggregates [6, 7], as well as colloidal rods [8] and other aspherical particles [9]. Applications for holographic particle characterization include monitoring protein aggregation in biopharmaceuticals [6], detecting agglomeration in semiconductor polishing slurries [10], gauging the progress of colloidal synthesis reactions [11, 12], performing microrheology [13], microrefractometry [14], and microporosimetry [15] measurements, assessing the quality of dairy products [16], and monitoring contaminants in wastewater [3].

The critical first step in holographic particle characterization is to identify features of interest within a recorded video frame, and to localize them well enough to enable subsequent analysis [17–19]. False positive and negative detections clearly are undesirable. Poor localization slows downstream analysis [19] and can prevent fitting algorithms from converging to reasonable results. Here, we demonstrate that machine-learning algorithms can meet the need for reliable feature detection and precise object localization in holographic video microscopy. With appropriate training, machine-learning algorithms surpass standard image-analysis techniques in their ability to cope with common image defects such as overlapping features. They also operate significantly faster, thereby enabling applications that need real-time performance on low-cost hardware.

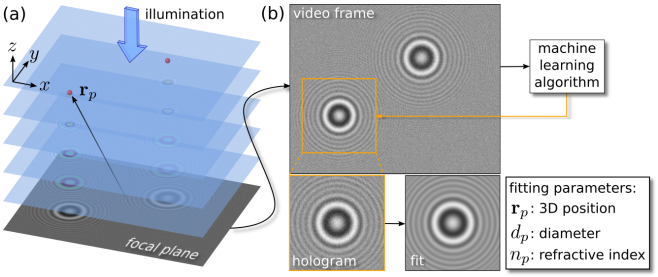

FIG. 1. Overview of holographic particle characterization. (a) Plane-wave illumination is scattered by colloidal particles (red spheres). The field scattered by a particle at $\mathbf{r}_p$ interferes with the plane wave to produce a hologram in the focal plane of a microscope. (b) Features in a digitally recorded hologram are detected with a machine learning algorithm before being analyzed with light-scattering theory to estimate the particles' physical properties.

DETECTING AND LOCALIZING HOLOGRAPHIC FEATURES

Figure 1 illustrates the challenge of recognizing features in holograms. Light scattered by a particle spreads as it propagates to the focal plane of a conventional microscope. There, it interferes with the remainder of the illuminating beam to create a pattern of concentric interference fringes. The microscope magnifies this interference pattern and projects it onto the detector of a video camera. The intensity variations associated with a single colloidal particle typically span many pixels in a recorded image and display rich internal structure. Their scale and complexity render such features difficult to recognize by

conventional particle-tracking techniques.

Heuristic Algorithms

One practical method for detecting holographic features and locating their centers involves transforming extended interference patterns into compact peaks [18, 19], and then locating the peaks with standard centroid detectors [17, 20]. Successful implementations of this approach have been based on circular Hough transforms [18, 20] and the orientational alignment transform (OAT) [19], both of which rely on typical holograms' radial symmetry without reference to the underlying image-formation mechanism.

Despite their demonstrated efficacy, these heuristic algorithms lack generality and tend to be computationally expensive. The range of contrast levels and feature sizes encountered in polydisperse and heterogeneous samples can confound algorithms that rely on empirically determined thresholds to distinguish features from background. The choice of image transformation limits what kinds of particles can be analyzed: an approach that reliably detects spheres may not work at all for colloidal clusters or rods. Overlapping features in multi-particle holograms similarly can confuse heuristic algorithms, even in otherwise ideal samples.

Machine Learning Algorithms

All of the above challenges and much of the processing can be mitigated with machine-learning techniques. We have implemented two such approaches: a cascade of boosted classifiers based on Haar-like wavelets, and a deep convolutional neural network (CNN). Both have particular strengths for particle localization in holographic microscopy images.

Cascade classifiers were originally developed for detecting faces in photographs [21]. They work by convolving an image with a sequence of selected wavelets and identifying regions with above-threshold response as candidate features. The training process determines which combination of wavelets contributes to each stage of the classification process. This approach has been adapted for a wide range of object recognition and image segmentation tasks [22]. Our application of this technique to holographic feature localization is based on an open-source implementation made available by the OpenCV project [23].

Convolutional neural networks also solve image recognition tasks through convolutions with selected kernels. In this case, the convolutions are integrated into the network's multi-layered, feed-forward architecture [24] and employ kernels that are designed and optimized during training. Constructing a CNN to perform general image classification requires massive computational resources [25]. Once constructed, however, a CNN can be retrained easily to recognize particular features of interest. Our application of CNNs for feature localization is based on TensorBox [26], an open-source package built on the GoogLeNet-OverFeat network [24].

Both types of supervised machine learning algorithms require sets of sample data for training and validation. Normally, these images are obtained experimentally and are annotated by hand. We instead train with synthetic holograms that are computed with the same light scattering theory used to analyze experimental holograms. Using the physics of image formation to provide the ground truth for training eliminates the effort and errors inherent in empirical annotation.

HOLOGRAPHIC IMAGE FORMATION

Referring to Fig. 1, we model the holographic microscope's illumination as a plane wave at frequency ω propagating down the $\hat{z}$ axis (along $-\hat{z}$) and linearly polarized along $\hat{x}$:

$$\mathbf{E}_0(\mathbf{r},t) = u_0\, e^{ikz} e^{i\omega t}\, \hat{x}, \tag{1}$$

where $k = n_m\omega/c$ is the wavenumber of the light in a medium of refractive index n_m. A particle at position $\mathbf{r}_p$ scatters the incident wave, thereby creating the scattered field

$$\mathbf{E}_s(\mathbf{r},t) = u_0\, e^{ikz_p}\, \mathbf{f}_s(k[\mathbf{r}-\mathbf{r}_p])\, e^{i\omega t}, \tag{2}$$

where $\mathbf{f}_s(k\mathbf{r})$ is the Lorenz-Mie scattering function [27, 28]. For the particular case of scattering by a sphere, $\mathbf{f}_s(k\mathbf{r})$ is parameterized by the sphere's radius a_p and refractive index n_p [27]. The field that reaches point $\mathbf{r}$ in the focal plane ($z = 0$) is the superposition of these two contributions,

$$\mathbf{E}(\mathbf{r},t) = \mathbf{E}_0(\mathbf{r},t) + \mathbf{E}_s(\mathbf{r},t). \tag{3}$$

The dimensionless intensity, $b(\mathbf{r}) \equiv u_0^{-2}\,|\mathbf{E}(\mathbf{r},t)|^2$, is then given by

$$b(\mathbf{r}) = \left|\hat{x} + e^{ikz_p}\, \mathbf{f}_s(k[\mathbf{r}-\mathbf{r}_p])\right|^2. \tag{4}$$

In addition to a_p and n_p, this model for the image formation process depends on a small number of parameters that characterize the instrument. Our holographic microscope is powered by a 15 mW fiber-coupled diode laser (Coherent Cube) operating at a vacuum wavelength of $\lambda = 447$ nm. The combination of a half-wave plate and a polarizing beam splitter reduces the power incident on the sample to 3 mW and ensures that the light is linearly polarized along $\hat{x}$, as required by Eq. (4). A 100× oil-immersion objective lens (Nikon S-Plan Apo, numerical

aperture 1.3) and a matched 200 mm tube lens provide a total magnification of 135 nm/pixel on a standard video camera (NEC TI-324AII). The 640 pixel × 480 pixel grid is digitized at 8 bits/pixel and recorded as uncompressed digital video at 29.97 frames/s with a commercial digital video recorder (Pioneer DVR-560H). The refractive index of the medium, n_m, is determined to within a part per ten thousand using an Abbe refractometer (Edmund Scientific).

Having determined the calibration constants, we treat the particle's position and properties as adjustable parameters and fit predictions of Eq. (4) to experimentally measured holograms. To do so, each video frame must first be corrected by subtracting off the camera's dark count [7], and then normalizing by the microscope's background intensity distribution [1]. Such fits typically yield a sphere's position with a precision of 1 nm in the plane and 3 nm axially [18, 29]. Characterization results are similarly precise, with the radius of a micrometer-diameter sphere typically being resolved to within 3 nm and the refractive index to within a part per thousand [14, 30].

This excellent performance requires starting estimates for the adjustable parameters that are good enough for the fitting algorithm to converge to a globally optimal solution. The fitter computes trial holograms according to Eq. (4), which is computationally expensive. It has to perform fewer of these computations when it is provided with better estimates for the starting parameters. Whereas heurstic localization algorithms meet this need, machine-learning algorithms are substantially faster and more robust, and can be comparably precise.

APPLYING MACHINE LEARNING TO HOLOGRAPHIC PARTICLE LOCALIZATION

We used Eq. (4) to generate training images of particles with radii ranging from $a_p = 0.25\,\mu\text{m}$ to $5\,\mu\text{m}$, refractive indexes from $n_p = 1.4$ to 2.5, and axial positions from $z_p = 5\,\mu\text{m}$ to $50\,\mu\text{m}$. Each training hologram has parameters selected at random from this range and is centered at random within the field of view. Normalized experimental holograms have uncorrelated white noise that we model as additive Gaussian noise with a standard deviation of five percent.

Our cascade classifier was trained with 6000 synthetic images of colloidal spheres. These were combined with a complementary set of 4000 negative images recorded by the instrument itself. The classifier was trained until its rate of false positive detections fell to 8×10^{-4}. This was achieved with a five-stage classifier composed of 5 sets of wavelets.

The convolutional neural network was trained with 3000 synthetic holographic images; another 600 were used for validation. To account for overlapping features, each computed hologram contains between zero and five randomly located particles with randomly selected properties. CNN training converged after 50 000 cycles of training and validation.

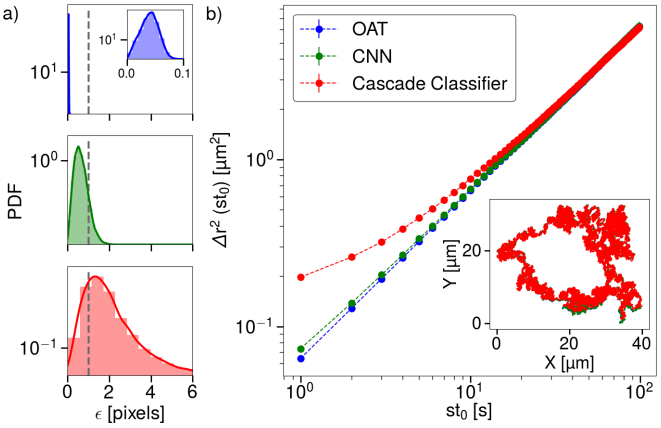

FIG. 2. Each localization technique provided estimates for the trajectory of a simulated brownian particle. (a) Probability distribution functions for the localization error achieved by (top) heuristic algorithm, (middle) convolutional neural network, and (bottom) cascade classifier. Inset shows expanded view of the subpixel resolution. Vertical dashed line indicated single-pixel precision. (b) Mean-square displacement computed from trajectories obtained with the three detection algorithms is shown. Short-time asymptotes yield dynamical estimates for the localization error.

Precision and Accuracy

We assess the detectors' localization precision by comparing detection results with known input parameters. A typical example for a particular choice of particle properties is shown in Fig. 2. The three probability distributions in Fig. 2(a) present the root-mean-square localization error obtained by each of the algorithms when tracking particles with $a_p = 1.0\,\mu\text{m}$ and $n_p = 1.5$. We generate data for these plots by simulating the diffusion of such a particle through water at a temperature of 20 °C starting from the center of the field of view at $z_p = 13.5\,\mu\text{m}$ and proceeding for 3000 steps at 33 ms per step.

The orientational alignment transform (OAT) consistently yields sub-pixel precision with a median error of 0.04 pixels. The convolutional neural network also yields sub-pixel precision with a median localization error of 0.61 pixels. The cascade classifier performs less well, with a median localization error of 1.81 pixels and a substantial probability for errors extending to several pixels. For applications such as Lorenz-Mie microscopy that require input estimates with sub-pixel precision, the cascade classifier's localization precision may not be sufficient.

The inset of Fig. 2(b) shows the trajectory reconstructed by each of the algorithms. The measured tra-

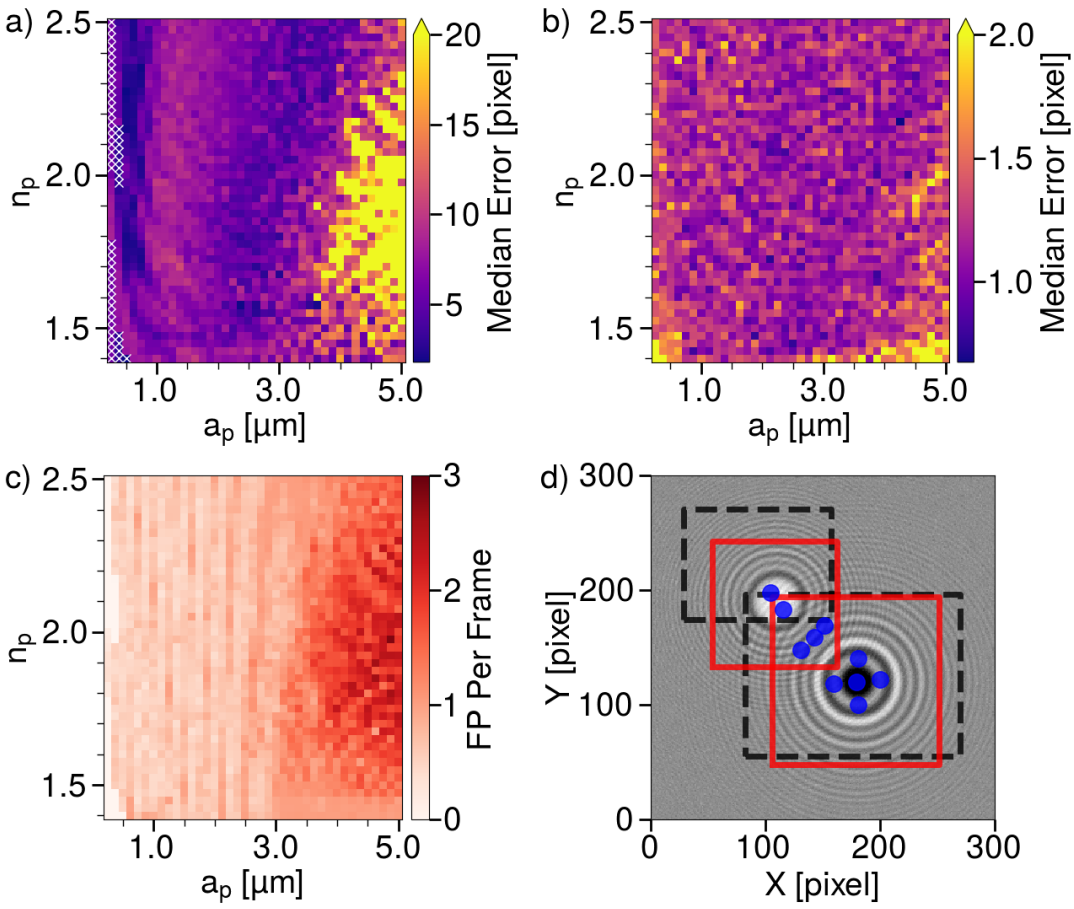

FIG. 3. Localization errors as a function of particle radius and refractive index at a height of $z_p = 13.5\,\mu\text{m}$ above the focal plane. (a) Cascade classifier. (b) Convolutional neural network. (c) Rate of false positive detections for the cascade classifier. (d) The resulting detections from each localization method over an example of overlapping holograms. The blue dots are the result for the orientational alignment transform; the red boxes for the CNN; the dashed-black boxes for the cascade classifier.

jectory's mean-squared displacement (MSD) provides an estimate for the particle's diffusion coefficient. All three methods yield results that are consistent with the particle's true diffusivity, $D = 0.482\,\mu\text{m}^2/\text{s}$, which suggests that their localization errors are normally distributed. Extrapolating the MSD to zero lag time provides an estimate for the localization error [17, 31]. In all three cases, the extrapolated measurement error is consistent with the median values from Fig. 2(a).

Applying the same techniques across the entire range of particle sizes and refractive indexes yields results for the median localization error summarized in Fig. 3(a) and 3(b). Results from the cascade classifer in Fig. 3(a) range from single-pixel precision under most conditions to more than 20 pixels for the largest spheres we considered. These errors are dominated by the cascade classifier's tendency to displace location estimates toward the center of the field of view when presented with features that extend outside the observation window. This problem is more pronounced for the larger holographic features created by larger scatterers. Smaller particles create holograms with low signal-to-noise ratio that can be overlooked by the cascade classifier, leading to false negative detections. Such conditions are indicated by white crosses in Fig. 3(a).

The results plotted in Fig. 3(b) show that CNN yields much smaller localization errors than the cascade classifier. The CNN achieves sub-pixel resolution over the entire range of parameters, although localization precision is worse for weak scatterers and large spheres. Unlike the cascade classifier, it also returned no false negative results.

Both the cascade classifier and the CNN return a small rate of false positive detections. Figure 3(c) reports the false-positive rate for the cascade classifier, which ranges from 10^{-1} /frame for holograms of particles with $a_p < 3\,\mu\text{m}$ to 3 /frame for holograms of larger spheres. In all cases, these false positive detections come in addition to the correct particle detection, and result from the classifier's failure to correct coalesce multiple detections of the same particle. Such false positive detections contribute to the very large localization error for large

spheres in Fig. 3(a). The CNN performs substantially better, with false positive rate less than 10^{-3} /frame over the entire range of parameters.

Multiple Particles

The results presented so far apply to holograms of single particles. In practice, it is not unusual for multiple particles to enter the microscope's field of view simultaneously. Interference between their scattering patterns create intensity variations that can confuse heuristic detection algorithms, particularly in the presence of noise. The two-particle hologram in Fig. 3(d) is a typical example. Discrete points overlaid on this image show the candidate positions identified for features in this hologram that were identified by the OAT heuristic algorithm. This image generated 8 false-positive detections, and incorrectly located one of the features off-center.

Both machine-learning algorithms perform better than the heuristic algorithm for overlapping features. The cascade classifier correctly detects both particles, as indicated by dashed rectangles in Fig. 3(d). The estimated locations, however, are displaced significantly from the features' true centers, presumably because of interference between the two scattering patterns. The CNN not only detects and localizes both particles correctly, but also provides useful estimates for the scattering patterns' extent, as denoted by the solid (red) squares overlaid on Fig. 3(d).

These results illustrate that machine learning algorithms can be more reliable than heuristic algorithms for detecting and localizing features in non-ideal holograms. For applications such as monitoring colloidal concentrations, this benefit alone might recommend machine-learning algorithms over the previous state of the art. The principal benefit of machine-learning algorithms, however, is their ability to detect features rapidly, even on low-power computational platforms.

Computation Speed

Table I presents timing data for holographic feature detection on a desktop workstation outfitted with an nVidia GTX 680 GPU. This system can detect a single feature in just under 700 ms using a python implementation of the OAT heuristic algorithm. The CNN routinely outperforms the heuristic algorithm by a factor of 2.5 on the same hardware. Transferring the CNN calculation to the GPU increases this advantage to a factor of 11. Most remarkably, the cascade classifier outperforms heuristic algorithms by a factor of 40, even without GPU acceleration, processing features fast enough to keep up with the 33 ms frame rate of a standard video camera.

The cascade classifier is so computationally efficient that it can be deployed usefully on a lightweight embedded computer. We demonstrated this by analyzing holograms on a Raspberry Pi 3 single-board computer. Even though the light-weight computer runs the cascade classifier 10 times slower than the workstation, it is still 4 times faster than the heuristic algorithms on the workstation. Reducing the resolution by half, improves the Raspberry Pi's detection time to 40 ms per image which corresponds to 25 frames/s.

Real-time detection of holographic features has applications beyond holographic particle characterization. The implementations presented here are suitable for targeting optical traps in holographic trapping systems [32]. We have demonstrated this by integrating machine-learning particle detection into an automated trapping system that projects optical traps onto the particles' positions to acquire them for subsequent processing. Unlike pioneering implementations of automated trapping [33] that rely on conventional imaging and so requires target particle to lie near the microscope's focal plane, holographic targeting works over a very large axial range. Both the CNN and the cascade classifier locate particles in the plane with sufficient precision to ensure reliable trapping. The axial coordinate required for three-dimensional targeting can be extracted from holographic features using previously reported techniques [2]. Because of its speed, the cascade classifier is particularly useful for targeting fast-moving particles. Figure 4 shows the cascade classifier tracking colloidal particles in real time as they diffuse in a holographic trapping system. The instrument then uses this tracking information to trap the detected particles, as shown in the associated video (Visualization 1).

DISCUSSION

The use of machine learning algorithms for detecting and localizing holographic features enable and enhane a host of applications for holographic video microscopy. CNNs detect and localize colloidal particles faster than conventional image-analysis techniques and localize particles well enough for subsequent processing. Our implementation also estimates the extent of each holographic feature thereby bypassing the standard next step in Lorenz-Mie microscopy [18] and saving additional time. These substantial speed enhancements make it possible to perform holographic particle characterization measurements in real time rather than requiring off-line processing. CNNs also are more successful at interpreting the overlapping holograms that arise in multi-particle holograms and thus can be used to analyze more concentrated suspensions.

The Haar-based cascade classifier also outstrips heuristic algorithms' ability to detect colloidal particles, par-

	Mean [ms]	Median [ms]	Std. [ms]	Min [ms]	Max [ms]
OAT (CPU)	695	700	11	670	1000
CNN (CPU)	278	278	2.8	271	32
CNN (GPU)	52	52	4.8	50	70
Cascade (CPU)	17	17	1.0	15	81
Cascade (RPi)	173	171	12	159	275

TABLE I. Analysis times in ms/frame for the OAT heuristic algorithm, the convolutional neural network (CNN) implemented on CPU and GPU, and the cascade classifier implemented on a workstation and on a Raspberry Pi 3 single-board computer.

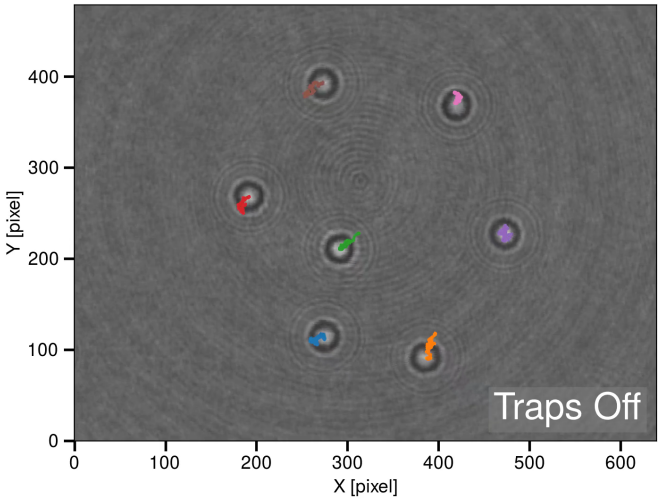

FIG. 4. Cascade classifier tracking 2 µm-diameter colloidal spheres diffusing through water in a holographic optical trapping system. Each trace shows 5 seconds of the associated particle's motion. The associated video (Visualization 1) shows the tracking data being used to alternately trap and release the particles.

ticularly in heterogeneous samples and crowded fields of view. Although it cannot match the tracking precision of CNNs, its speed and modest computational requirements create new opportunities. We have deployed our cascade classifier on a light-weight single-board computer and have demonstrated its utility for counting particles and thus for measuring colloidal concentrations. Such a low-cost instrument should be useful for routine monitoring of industrial processes and products and for environmental monitoring. We also have demonstrated the cascade classifier's utility for high-speed targeting in holographic trapping. In this case, speed is more important than tracking precision for interacting with processes as they unfold.

While the present study focuses on detecting and localizing holographic features with radial symmetry, the machine-learning framework can be applied equally well to asymmetric holograms produced by rods, clusters or biological samples. By reducing the computational burden of analyzing holograms, machine learning algorithms extend the reach of holographic tracking and holographic characterization. More generally, machine-learning algorithms are well-suited to bootstrapping the more detailed analysis involved in holographic particle characterization. We anticipate that more of these physics-based processing steps will be taken over by machine-learning algorithms as that technology advances.

ACKNOWLEDGEMENTS

This work was supported primarily by the MRSEC program of the National Science Foundation through Award no. DMR-1420073 and in part by the SBIR program of the NSF through Award no. IPP-1519057. The holographic trapping instrument was developed under the MRI program of the NSF through Grant Number DMR-0922680. Software for holographic particle tracking and characterization is available online at `https://github.com/davidgrier/`.

[1] S.-H. Lee, Y. Roichman, G.-R. Yi, S.-H. Kim, S.-M. Yang, A. van Blaaderen, P. van Oostrum, and D. G. Grier, "Characterizing and tracking single colloidal particles with video holographic microscopy," Opt. Express **15**, 18275-18282 (2007).

[2] A. Yevick, M. Hannel, and D. G. Grier, "Machine-learning approach to holographic particle characterization," Opt. Express **22**, 26884-26890 (2014).

[3] L. A. Philips, D. B. Ruffner, F. C. Cheong, J. M. Blusewicz, P. Kasimbeg, B. Waisi, J. R. McCutcheon, and D. G. Grier, "Holographic characterization of contaminants in water: Differentiation of suspended particles in heterogeneous dispersions," Water Res. **122**, 431-439 (2017).

[4] R. W. Perry, G. Meng, T. G. Dimiduk, J. Fung, and V. N. Manoharan, "Real-space studies of the structure and dynamics of self-assembled colloidal clusters," Faraday Discuss. **159**, 211-234 (2012).

[5] J. Fung, and V. N. Manoharan, "Holographic measurements of anisotropic three-dimensional diffusion of colloidal clusters," Phys. Rev. E **88**, 020302 (2013).

[6] C. Wang, X. Zhong, D. B. Ruffner, A. Stutt, L. A. Philips, M. D. Ward, and D. G. Grier, "Holographic characterization of protein aggregates," J. Pharm. Sci. **105**, 10741085 (2016).

[7] C. Wang, F. C. Cheong, D. B. Ruffner, X. Zhong, M. D. Ward, D. G. Grier, "Holographic characterization of

colloidal fractal aggregates," Soft Matter **12**, 8774-8780 (2016).

[8] F. C. Cheong and David G. Grier, "Rotational and translational diffusion of copper oxide nanorods measured with holographic video microscopy," Opt. Express **18**, 65556562 (2010).

[9] M. Hannel, C. Middleton, and D. G. Grier, "Holographic characterization of imperfect colloidal spheres," Appl. Phys. Lett. **107**, (2015).

[10] F. C. Cheong, P. Kasimbeg, D. B. Ruffner, E. H. Hlaing, J. Blusewicz, L. A. Philips, and D. G. Grier, "Holographic characterization of colloidal particles in turbid media," Appl. Phys. Lett. **111**, 153702 (2017).

[11] C. Wang, H. Shpaisman, A. D. Hollingsworth, and D. G. Grier, "Celebrating Soft Matter's 10th Anniversary: Monitoring colloidal growth with holographic microscopy," Soft Matter **11**, 1062-1066 (2015).

[12] C. Wang, H. W. Moyses, and D. G. Grier, "Stimulus-responsive colloidal sensors with fast holographic readout," Appl. Phys. Lett. **107**, 051903 (2015).

[13] F. C. Cheong, S. Duarte, S. H. Lee, and D. G. Grier, "Holographic microrheology of polysaccharides from *Streptococcus mutans* biofilms," Rheol. Acta **48**, 109-115 (2009).

[14] H. Shpaisman, B. J. Krishnatreya, and D. G. Grier, "Holographic microrefractometer," Appl. Phys. Lett. **101**, 091102 (2012).

[15] F. C. Cheong, K. Xiao, D. Pine, and D. G. Grier, "Holographic characterization of individual colloidal spheres' porosities," Soft Matter **7**, 6816-6819 (2011).

[16] F. C. Cheong, K. Xiao, and D. G. Grier, "Technical Note: Characterizing individual milk fat globules with holographic video microscopy," J. Dairy Sci. **92**, 95-99 (2009).

[17] J C. Crocker, D G. Grier, "Methods of digital video microscopy for colloidal studies," J. Colloid Interface Sci. **179**, 298-310 (1996).

[18] F. C. Cheong, B. Sun, R. Dreyfus, J. Amato-Grill, K. Xiao, L. Dixon, and D. G. Grier, "Flow visualization and flow cytometry with holographic video microscopy," Opt. Express **17**, 13071-13079 (2009).

[19] B. J. Krishnatreya and D. G. Grier, "Fast feature identification for holographic tracking: The orientation alignment transform," Opt. Express **22**, 1277312778 (2014).

[20] D. Allan,, T. Caswell, N. Keim, and C. van der Wel, "Trackpy v0.3.2", `http://doi.org/10.5281/zenodo.60550`.

[21] P. Viola and M. Jones, "Rapid object detection using a boosted cascade of simple features," in *IEEE Proceedings on Computer Vision and Pattern Recognition* (IEEE, 2001), Vol.1, pp 511-518.

[22] R. Lienhart and J. Maydt, "An extended set of Haar-like features for rapid object detection," in *IEEE Proceedings on Image Processing* (IEEE, 2002), Vol.1, pp 900-903.

[23] Itseez, "Open source computer vision library," `https://github.com/itseez/opencv`.

[24] P. Sermanet, D. Eigen, X. Zhang, M. Mathieu, R. Fergus, and Y. Lecun, "OverFeat: Integrated recognition, localization and detection using convolutional networks," International Conference on Learning Representations (ICLR) (2015).

[25] M. Abadi, A. Agarwal, P. Barham, E. Brevdo, Z. Chen, C. Citro, G. S. Corrado, A. Davis, J. Dean, M. Devin, S. Ghemawat, I. Goodfellow, A. Harp, G. Irving, M. Isard, Y. Jia, R. Jozefowicz, L. Kaiser, M. Kudlur, J. Levenberg, D. Mane, R. Monga, S. Moore, D. Murray, C. Olah, M. Schuster, J. Shlens, B. Steiner, I. Sutskever, K. Talwar, P. Tucker, V. Vanhoucke, V. Vasudevan, F. Viegas, O. Vinyals, P. Warden, M. Wattenberg, M. Wicke, Y. Yu, and X. Zheng, "Tensorflow: Large-scale machine learning on heterogeneous distributed systems," arXiv:1603.04467 (2016).

[26] R. Stewart and M. Andriluka, "End-to-end people detection in crowded scenes," arXiv:1506.04878 (2015).

[27] C. F. Bohren and D. R. Huffman, *Absorption and Scattering of Light by Small Particles* (Wiley Interscience, 1983).

[28] M. I. Mishchenko, L. D. Travis, and A. A. Lacis, *Scattering, Absorption and Emission of Light by Small Particles* (Cambridge University Press, Cambridge, 2001).

[29] F. C. Cheong, B. J. Krishnatreya, and D. G. Grier, "Strategies for three-dimensional particle tracking with holographic video microscopy," Opt. Express **18**, 13563-13573 (2010).

[30] B. J. Krishnatreya, A. Colen-Landy, P. Hasebe, B. A. Bell, J. R. Jones, A. Sunda-Meya, and D. G. Grier, "Measuring Boltzmann's constant through holographic video microscopy of a single sphere," Am. J. Phys. **82**, 2331 (2014).

[31] X. Michalet and A. J. Berglund, "Optimal diffusion coefficient estimation in single-particle tracking," Phys. Rev. E **85**, 061916 (2012).

[32] D. G. Grier, "A revolution in optical manipulation", Nature **424**, 810-816 (2003).

[33] S. C. Chapin, V. Germain and E. R. Dufresne, "Automated trapping, assembly, and sorting with holographic optical tweezers," Opt. Express **14**, 13096-13100 (2006).